

Truncated Wigner approximation for the bosonic model of large spin bathsMohsen Yarmohammadi ^{1,2,*}, Katrin Bolsmann,^{2,†} Yvonne Ribbeheger,^{2,‡} Timo Gräßer ^{2,§} and Götz S. Uhrig ^{2,||}¹*Department of Physics, The University of Texas at Dallas, Richardson, Texas 75080, USA*²*Condensed Matter Theory, TU Dortmund University, Otto-Hahn Straße 4, 44221 Dortmund, Germany*

(Received 21 January 2023; revised 10 March 2023; accepted 17 March 2023; published 24 March 2023)

The central spin model has a wide applicability. It is ideally suited to describe a small quantum system, for instance a quantum bit, in contact to a bath of spins, e.g., nuclear spins or other small quantum systems in general. According to previous work [R. Röhrig *et al.*, *Phys. Rev. B* **97**, 165431 (2018)], a large bath of quantum spins can be described as a bath of quantum harmonic oscillators. But the resulting quantum model is still far from being straightforwardly solvable. Hence we consider a chain representation for the bosonic degrees of freedom to study how well a semi-classical truncated Wigner approximation of the effective model of harmonic oscillators (bTWA) works in comparison with other approximate and exact methods. We find that the bTWA works well for short times, but deviates from the results of other methods for long times. The general message is that the applicability of semi-classical approaches strongly depends on the variables in terms of which the model is formulated. Numerically, we examine the effect of the number of bath spins and of the truncation level, i.e., the chain length.

DOI: [10.1103/PhysRevB.107.125421](https://doi.org/10.1103/PhysRevB.107.125421)**I. INTRODUCTION**

The central spin model (CSM) is a well-known model describing the interaction of a single “central” spin with surrounding spins [1,2], for instance, the interaction of the spin of a localized electron with nuclear spins in quantum dots [3–5]. In view of the intense search for physical realizations of quantum bits [6], a localized electron in a quantum dot can be seen as a two-level system and thus as a promising candidate for quantum bits [7–9]. The CSM is a quantum many-body system and major progress has been made to understand its properties in its applications for phenomena in material science and quantum information technology [10–13]. Polarization recovery in a longitudinal field [14,15], nuclei-induced frequency focusing [16–18], spin precession mode locking [19,20], the effect of spin inertia [21,22], spin noise [23–27], and many other effects belong to the particularly rich physics of the CSM. Furthermore, the CSM is also used to understand the dynamics of quantum sensors [28] which helps to reach high sensitivities.

For a finite, not too large number of bath spins [29], it is possible to use the Bethe ansatz [1,30,31] to diagonalize the CSM Hamiltonian and to analyze rigorous restrictions of the central spin dynamics stemming from conserved quantities [32,33]. If all couplings are equal the CSM reduces to the so-called *box model* allowing one to compute the spin dynamics for large spin baths essentially analytically [34–36]. However,

the complexity of the CSM in practical applications is related mainly to the electron spin decoherence when interacting with an (almost) infinite number of nuclei spins [5,37–42]. In this scenario, the initial polarization and information on the spin state is quickly and irreversibly lost.

To describe this decoherence of the central spin and to conceive strategies against it, various approaches have been conceived. Density-matrix renormalization group (DMRG) deals with up to 1000 spins, but only up to relatively short times [43,44] due to the fast growth of entanglement. The linked-cluster and cluster-correlation expansions [45–48] investigate the long-time spin decoherence, but of finite, relatively small spin baths. Moreover, considering the nuclear-electric quadrupolar interactions for a few spins, the spin-noise spectrum at various timescales has been calculated using Chebyshev polynomials [27,49,50]. Furthermore, a coherent interface between electron and nuclear spins was recently developed [51] with the vision to realize long-lived quantum memory.

Although a classical description of CSM with a large-enough number of nuclear spins can be justified over a long time, it neglects all quantum mechanical aspects [43,44] which are vital for quantum bits. This originates from the fact that the central spin is a truly quantum mechanical object and its back-action on the bath spins is not classical. The truncated Wigner approximation (TWA) [52] is a general semi-classical approach in which quantum fluctuations are partly taken into account through random initial conditions for the classical equations of motion. Although the equations of motion themselves are still purely classical, correlations and the probabilities of quantum measurements can be simulated to a certain degree. The TWA has often been used to simulate the dynamics of the CSM [10,44,53–55]. The spins are taken as classical vectors precessing around local classical fields.

*mohsen.yarmohammadi@utdallas.edu

†katrin.bolsmann@tu-dortmund.de

‡yvonne.ribbeheger@tu-dortmund.de

§timo.graesser@tu-dortmund.de

||goetz.uhrig@tu-dortmund.de

We abbreviate this semi-classical approach to spins sTWA. It can be implemented for a moderate numbers of spins ($N \approx 200$) if one has to simulate long times. Experimentally, the bath sizes range from 10^4 to 10^6 still exceeding numerical resources by far even though a hierarchical chain representation based on generalized Overhauser fields helps to reconcile large spin baths and long-time simulations [54].

In this framework, a fully quantum mechanical approach [56] based on iterated equations of motion (iEoM) has been suggested for large spin baths. The advantage of this approach is that it is particularly suited to capture very large or even infinitely large spin baths. The bath of spins is mapped to a bath of hierarchically coupled bosons and the central spin is mapped to a four-dimensional impurity. But the fully quantum mechanical evaluation of the dynamics of the effective bosonic model for long times represents still a tremendous challenge. Hence, it is interesting to study approximate ways to treat this effective bosonic model.

In this work, we study the application of the TWA to the mapped effective bosonic model resulting from iEoM [56], i.e., to the harmonic oscillators. The impurity is described by two spins with $S = 1/2$ which, in turn, are treated as classical vectors. To distinguish this TWA from the one resulting from the classical treatment of the spins we call it bosonic TWA (bTWA). Clearly, the bTWA would remove the restrictions on the maximum number of bosonic modes which can be simulated. The immediate aim is to describe the experimental spin-noise spectra [26,57,58]. To benchmark the bTWA, we compare our data to data from some of the above-mentioned techniques under the same conditions.

This paper is organized as follows. In Sec. II, we review the CSM and in Sec. III, we present its bosonic formulation. In Sec. IV, we present our results and compare them with results from other techniques. Finally, the paper is summarized in Sec. V.

II. INITIAL MODEL

In this section, we briefly introduce the CSM. For our proof-of-principle study, we restrict ourselves to the paradigmatic isotropic version of the CSM. This implies that we neglect dipole-dipole interaction [38,59], quadrupolar couplings [49,60–63], and spin-orbit couplings [64–68] of the nuclear spins which usually become relevant on very long timescales. We start with the CSM comprising a central spin \hat{S}_0 with $S = 1/2$ interacting through the hyperfine coupling with a bath of N spins \hat{S}_ℓ . The Hamiltonian reads

$$\hat{\mathcal{H}} = \sum_{\ell=1}^N J_\ell \hat{S}_0 \cdot \hat{S}_\ell, \quad (1)$$

where J_ℓ denotes the hyperfine coupling of the ℓ th spin in the bath. In electronic quantum dots, the coupling constants J_ℓ are proportional to the probability that the electron is present at the site of the nucleus ℓ [38,59], which is given by the modulus squared of the electronic wave function. It is convenient to define a composite field for the effect of the bath spins, $\hat{B} = \sum_{\ell=1}^N J_\ell \hat{S}_\ell$, which is called the Overhauser field.

With its help, the Hamiltonian can simply be rewritten as $\hat{\mathcal{H}} = \hat{S}_0 \cdot \hat{B}$.

Let us consider an infinite spin bath ($N \rightarrow \infty$) with decreasing couplings. We consider the generic parametrization $J_\ell = C \exp(-\ell\gamma)$ [16,30,31,33,54] with $\ell \in \{1, 2, \dots, N\}$, where the prefactor C sets the energy scale. For $\gamma > 0$, the exponential term is decreasing with ℓ . The meaning of γ is elucidated by the following argument. Even if $N \rightarrow \infty$, there is only a finite number of bath spins which is appreciably coupled to the central spin. We denote this number by N_{eff} and define it by the ratio of the squared sum of all couplings and the sum of all squared couplings [38,43,44,54,59,69], i.e., $N_{\text{eff}} := (\sum_{\ell=1}^N J_\ell)^2 / J_Q^2$, where $J_Q^2 := \sum_{\ell=1}^N J_\ell^2$. Inserting our parametrization J_ℓ into N_{eff} in the limit $N \rightarrow \infty$, we find for small values γ

$$N_{\text{eff}} = \frac{2}{\gamma} + \mathcal{O}(\gamma). \quad (2)$$

So γ is about twice the inverse number of effectively coupled spins. The electron spin in quantum dots is coupled to a very large number of bath spins [38,59,70,71], $N_{\text{eff}} \approx 10^4$ to 10^6 , so, $\gamma \approx 10^{-4}$ to 10^{-6} is a realistic estimate. Moreover, we set the energy scale for all simulations by requiring $J_Q = 1$. This results in $C \simeq \sqrt{2\gamma} \approx 10^{-2}$ to 10^{-3} , which is a very small number implying that the contribution of an individual bath spin is negligible. Only suitable sums over all spins have a sizable impact. In contrast, for large γ , we deal with a small number of bath spins, see Eq. (2), and the dynamics of the central spin can be determined using fully quantum mechanical descriptions [27,48,49].

III. EFFECTIVE MODEL AND SEMI-CLASSICAL APPROACH

In what follows, we sketch the mapping of the spin bath on a bosonic bath (iEoM [56]). Then, we introduce the semi-classical approach bTWA based on a hierarchical chain representation to describe the *long-time* spin dynamics.

A. Objective

We begin with the application of the Heisenberg equation of motion to the CSM, $\partial_t \hat{A} = i[\hat{\mathcal{H}}, \hat{A}]$ (throughout the present work, \hbar is set to unity), where \hat{A} are operators of the CSM forming a suitable operator basis for the products of all components of spin operators at all sites [56]. In the end, we are interested in the α -component of the spin-spin autocorrelation function of the central spin at infinite temperature

$$S^\alpha(t) = \langle \hat{S}_0^\alpha(t) \hat{S}_0^\alpha(0) \rangle, \quad (3)$$

for small values of the parameter γ corresponding to large spin baths.

The spin bath is taken to be in the completely disordered state initially. In particular, the long-term behavior of $S^\alpha(t)$ provides information about the fate of state with the central spin aligned along the z -axis initially, i.e., at $t = 0$. Assuming infinite temperature is well justified because the thermal energy in the bath at temperatures of a few Kelvin is at least one order of magnitude larger than the individual couplings in a quantum dot [72].

For motivation, we provide the autocorrelation if a constant external or internal classical magnetic field is applied [38,43]

$$\begin{aligned} \hat{S}_0(t) = & \bar{n}[\bar{n} \cdot \hat{S}_0(0)] + \{\hat{S}_0(0) - \bar{n}[\bar{n} \cdot \hat{S}_0(0)]\} \cos(Bt) \\ & - [\bar{n} \times \hat{S}_0(0)] \sin(Bt), \end{aligned} \quad (4)$$

where \bar{n} points in the direction of the magnetic field $B = |\bar{B}|$. This formula is identical to the classical one since \bar{B} is a classical vector and the equations of motion are linear in the spin operators so that the Ehrenfest theorem states that the equations of motion of the operators or their expectation values are identical to the ones of the corresponding classical variables. Obviously, powers of B up to infinite order occur so that a suitable operator basis needs operators including high powers of the Overhauser field if we want to capture its intrinsic quantum character and the ensuing dynamics.

If one neglects the dynamics of the Overhauser field completely, the frozen Overhauser field approximation is retrieved for which one averages over all random directions and random strengths of the Overhauser field [38,43] yielding

$$S^\alpha(t) = \frac{1}{12} [2e^{-J_Q^2 t^2/8} (1 - J_Q^2 t^2/4) + 1]. \quad (5)$$

This analytic result is convenient as reference, see the figures below.

B. Effective model with higher powers of the Overhauser field

The orthogonal Hermite polynomials of the Overhauser field and similar composite weighted sums of the bath spin were introduced by Röhrig *et al.* [56] as a suitable operator basis. These polynomials are orthogonal for a Gaussian weight function [73] and can be applied to different components of generalized Overhauser fields by the recursive relation

$$\hat{G}_j^\alpha H_n(\hat{G}_j^\alpha) = \sqrt{n} H_{n-1}(\hat{G}_j^\alpha) + \sqrt{n+1} H_{n+1}(\hat{G}_j^\alpha), \quad (6)$$

where $\alpha = \{x, y, z\}$ and $H_0(\hat{G}_j^\alpha) = 1$ by definition. The polynomials $H_n(\hat{G}_j^\alpha)$ are the Hermite polynomials of degree n in the generalized Overhauser field vectors \hat{G} . These fields are defined by

$$\hat{G}_j^\alpha := 2 \sum_{\ell=1}^N \mathcal{P}_j(J_\ell) \hat{S}_\ell^\alpha, \quad (7)$$

where the real orthogonal polynomials $\mathcal{P}_j(x)$ are defined such that they comply with the orthogonality relation [54,56]

$$\delta_{j,m} = \sum_{\ell=1}^N \mathcal{P}_j(J_\ell) \mathcal{P}_m(J_\ell). \quad (8)$$

The polynomials $\mathcal{P}_j(J_\ell)$ describe the weight of each bath spin \hat{S}_ℓ .

In Eq. (1), we deal with the usual Overhauser field $\hat{B} = \sum_{\ell=1}^N J_\ell \hat{S}_\ell$, while in Eq. (7), generalized Overhauser field vectors \hat{G}_j are implemented. They arise hierarchically in their equations of motion: the time derivative of \hat{G}_j requires \hat{G}_{j+1} and so on. To find the orthonormal polynomials, we use the

standard Lanczos procedure

$$x \mathcal{P}_j(x) = \eta_j \mathcal{P}_{j+1}(x) + \chi_j \mathcal{P}_j(x) + \eta_{j-1} \mathcal{P}_{j-1}(x), \quad (9)$$

where $\mathcal{P}_0(x) = 0$, $\mathcal{P}_1(x) = x$ and χ_j, η_j are the usual recursion coefficients of the orthonormal polynomials for the scalar product (8). Hence, we obtain $\hat{G}_1 = 2\hat{B}$, meaning that the first generalized Overhauser field is twice the usual Overhauser field, where the factor of 2 is just needed for the orthonormalization of polynomials. The generalized Overhauser fields use orthonormal polynomials instead of simple powers because the latter would yield highly unstable equations upon truncation [54].

The established EoM for this basis of operators tells us that a single $H_n(G_j^\alpha)$ is transformed into the terms $\sqrt{n} H_{n-1}(G_j^\alpha)$ and $\sqrt{n+1} H_{n+1}(G_j^\alpha)$. This is identical to the effect of an annihilation (\hat{a}) and creation (\hat{a}^\dagger) bosonic operator, respectively, applied to the eigenstates $|n\rangle$ of a harmonic oscillator.

Eventually, a quantum mechanical representation of large spin baths by means of the iEoM for the generalized Overhauser fields including an external magnetic field has been obtained and developed, see Ref. [56] for further details. It is shown that in the limit $N \rightarrow \infty$ the isotropic CSM can be mapped onto a four-dimensional impurity coupled to a noninteracting bosonic bath yielding the effective Hamiltonian $\hat{\mathcal{H}}_{\text{eff}} = \hat{\mathcal{H}}_{\text{eff}}^{\text{CS}} + \hat{\mathcal{H}}_{\text{eff}}^{\text{ch}} + \hat{\mathcal{H}}_{\text{eff}}^{\text{Z}}$ in the presence of an external Zeeman magnetic field h along the z -direction. It is given by

$$\hat{\mathcal{H}}_{\text{eff}}^{\text{CS}} = \frac{1}{2} \sum_{\alpha=1}^3 \hat{K}_\alpha (\hat{a}_{1,\alpha}^\dagger + \hat{a}_{1,\alpha}), \quad (10a)$$

$$\begin{aligned} \hat{\mathcal{H}}_{\text{eff}}^{\text{ch}} = & \frac{i}{2} \sum_{j=1}^{N_{\text{tr}}} \sum_{\alpha,\beta,\delta=1}^3 \epsilon_{\alpha\beta\delta} \hat{M}_\beta [\chi_j \hat{a}_{j,\delta}^\dagger \hat{a}_{j,\alpha} \\ & + \eta_j (\hat{a}_{j+1,\delta}^\dagger \hat{a}_{j,\alpha} - \hat{a}_{j,\alpha}^\dagger \hat{a}_{j+1,\delta})], \end{aligned} \quad (10b)$$

$$\hat{\mathcal{H}}_{\text{eff}}^{\text{Z}} = -h \hat{K}_z, \quad (10c)$$

where $\hat{\mathcal{H}}_{\text{eff}}^{\text{CS}}$ refers to the central spin located at the head of a bosonic chain, whereas $\hat{\mathcal{H}}_{\text{eff}}^{\text{ch}}$ acts on a bosonic chain with flavors α as depicted in Fig. 1. In the above equations, $\epsilon_{\alpha\beta\delta}$ is the Levi-Civita tensor. The couplings η_j and χ_j result from the recursion of the orthogonal polynomials \mathcal{P}_j which can be expressed in the matrix form

$$\hat{\mathcal{T}} = \begin{pmatrix} \chi_1 & \eta_1 & 0 & 0 & \cdots \\ \eta_1 & \chi_2 & \eta_2 & 0 & \cdots \\ 0 & \eta_2 & \chi_3 & \eta_3 & \cdots \\ \vdots & \vdots & \ddots & \ddots & \ddots \end{pmatrix}, \quad (11)$$

with $J_\ell \mathcal{P}_j(J_\ell) = \hat{\mathcal{T}} \mathcal{P}_j(J_\ell)$ using the vector of polynomials $\mathcal{P}_j(J_\ell) = [\mathcal{P}_1(J_\ell), \mathcal{P}_2(J_\ell), \dots, \mathcal{P}_n(J_\ell)]^\top$. By definition, we have $\eta_0 = 0$. While the chain is half-infinite for an infinite bath, it is truncated at j_{max} in practical calculations [54,56] so that we also have $\eta_{j_{\text{max}}} = 0$. (In Ref. [54], the truncation level was denoted by $N_{\text{tr}} = j_{\text{max}}$.)

The commutation and anticommutation of the operators of the central spin with $\hat{\sigma}_\alpha$ (Pauli matrices) in the chain are

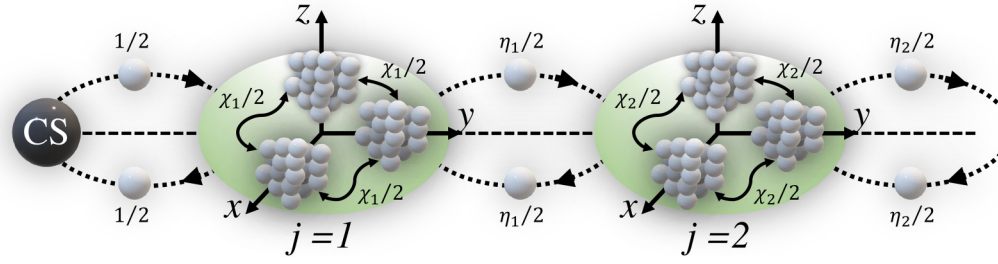


FIG. 1. Sketch of the CSM described by Eqs. (10a) and (10b). The central spin and the bosons in the chain are shown by the black and light gray solid spheres, respectively. The solid two-sided arrows inside the boxes illustrate the couplings $\chi_j/2$ between bosons of different flavors at the same site of the chain, while the dotted ones indicate the couplings $\eta_j/2$ between bosons on adjacent sites.

expressed by the matrices \hat{K}_α and \hat{M}_α with $\alpha \in \{x, y, z\}$, respectively, with matrix elements

$$\begin{aligned} \langle\langle n | \hat{K}_\alpha | m \rangle\rangle &= \frac{1}{2} \langle\langle \hat{\sigma}_n | [\hat{\sigma}_\alpha, \hat{\sigma}_m] \rangle\rangle \\ &= \begin{cases} 0 & \text{if } nm = 0, \\ i\epsilon_{\alpha\beta\delta} & \text{otherwise,} \end{cases} \end{aligned} \quad (12a)$$

$$\begin{aligned} \langle\langle n | \hat{M}_\alpha | m \rangle\rangle &= \frac{1}{2} \langle\langle \hat{\sigma}_n | \{\hat{\sigma}_\alpha, \hat{\sigma}_m\} \rangle\rangle \\ &= \begin{cases} \delta_{n,\alpha} + \delta_{m,\alpha} & \text{if } nm = 0, \\ i\epsilon_{\alpha\beta\delta} & \text{otherwise,} \end{cases} \end{aligned} \quad (12b)$$

for $\{m, n\} \in \{0, x, y, z\}$. Note that $\hat{M}_0 = \hat{I}_{4 \times 4}$ and $\hat{K}_0 = \hat{O}_{4 \times 4}$. The notation $\langle\langle \dots \rangle\rangle$ is used for the scalar product of operators for which we use $\langle\langle \hat{A} | \hat{B} \rangle\rangle := \langle \hat{A}^\dagger \hat{B} \rangle_{T=\infty}$, i.e., the expectation value at infinite temperature. Straightforwardly, we find

$$\hat{K}_\alpha = i \begin{pmatrix} 0 & 0 & 0 & 0 \\ 0 & 0 & \delta_{\alpha,z} & -\delta_{\alpha,y} \\ 0 & -\delta_{\alpha,z} & 0 & \delta_{\alpha,x} \\ 0 & \delta_{\alpha,y} & -\delta_{\alpha,x} & 0 \end{pmatrix}, \quad (13a)$$

$$\hat{M}_\alpha = \begin{pmatrix} 0 & \delta_{\alpha,x} & \delta_{\alpha,y} & \delta_{\alpha,z} \\ \delta_{\alpha,x} & 0 & 0 & 0 \\ \delta_{\alpha,y} & 0 & 0 & 0 \\ \delta_{\alpha,z} & 0 & 0 & 0 \end{pmatrix}. \quad (13b)$$

We emphasize that the chain Hamiltonian $\hat{\mathcal{H}}_{\text{eff}}^{\text{ch}}$ induces only a slow dynamics because the coupling between the head of the chain and its next site is $J_Q = 1$, while the coupling between different chain sites as well as the hopping processes between different flavors at each site is of order $\sqrt{\gamma}J_Q \approx 10^{-2}$ to 10^{-3} . Therefore, the quantum effects such as the dynamics in the bath and eventually dephasing and relaxation of the polarization of the central spin due to the presence of the bath of spins is slow.

Finally, we state that the autocorrelation expressed by the derived effective model reads

$$S^\alpha(t) = \frac{1}{4} \langle e_\alpha, \mathbf{0} | e^{-i\hat{\mathcal{H}}_{\text{eff}}^{\text{ch}}} | e_\alpha, \mathbf{0} \rangle, \quad (14)$$

with $e_\alpha = (0, \delta_{\alpha,x}, \delta_{\alpha,y}, \delta_{\alpha,z})^\top$ and $\mathbf{0}$ being the vacuum of all bosons. The autocorrelation (14) can be reformulated with the

help of the matrix \hat{M}_α and $e_1 = (1, 0, 0, 0)^\top$

$$S^\alpha(t) = \frac{1}{4} \langle e_1, \mathbf{0} | \hat{M}_\alpha e^{-i\hat{\mathcal{H}}_{\text{eff}}^{\text{ch}}} \hat{M}_\alpha | e_1, \mathbf{0} \rangle \quad (15a)$$

$$= \frac{1}{4} \langle e_1, \mathbf{0} | e^{i\hat{\mathcal{H}}_{\text{eff}}^{\text{ch}}} \hat{M}_\alpha e^{-i\hat{\mathcal{H}}_{\text{eff}}^{\text{ch}}} \hat{M}_\alpha | e_1, \mathbf{0} \rangle \quad (15b)$$

$$= \frac{1}{4} \langle e_1, \mathbf{0} | \hat{M}_\alpha(t) \hat{M}_\alpha(0) | e_1, \mathbf{0} \rangle, \quad (15c)$$

where we used the fact that $\hat{\mathcal{H}}_{\text{eff}}^{\text{ch}} | e_1, \mathbf{0} \rangle = 0$ since $\hat{K}_\alpha e_1 = 0$ and all bosonic terms in the chain part annihilate the bosonic vacua.

C. Bosonic truncated Wigner approximation

Generally, the TWA is a semi-classical approach based on the Wigner-Weyl quantization of the phase space [52]. It describes the quantum mechanical evolution of expectation values by computing classical trajectories in phase space for quasiprobability distributions, the so-called Wigner functions, of initial conditions. These distributions reflect the quantum mechanical uncertainty in the knowledge of the initial expectation values: the values of position and momentum or of the different components of angular momentum cannot be known exactly. The classical trajectories can be motivated by Feynman's path-integral formalism: the stationarity of the phase along these trajectories implies that they contribute the most to the temporal evolution.

To set up a TWA we need a set of observables of which we want to track the expectation values. For these, the equations of motion are derived and then approximated by their classical counterparts similar to the Ehrenfest theorem. For spins, this was nicely described in Ref. [55]. The initial distributions can often be taken to be normal distributions although this is not rigorously true, but successful in practice [53]. Since the Ehrenfest theorem becomes exact for bilinear bosonic Hamiltonians or linear spin Hamiltonian the TWA becomes exact in these cases.

To apply a TWA to the effective model defined in the previous section we need to represent the four-dimensional impurity by objects which have classical counterparts. Here we choose two spins with $S = 1/2$ which together span a four-dimensional Hilbert space. We denote their singlet state by $|s\rangle$ and their three triplet states by $|t_\alpha\rangle$ for $\alpha \in \{x, y, z\}$, identified with the four-dimensional Cartesian vectors $|s\rangle = (1 \ 0 \ 0 \ 0)^\top$ and $|t_\alpha\rangle = (0 \ \delta_{\alpha x} \ \delta_{\alpha y} \ \delta_{\alpha z})^\top$. Elemen-

tary linear algebra [74] yields the action of the spin operators on these states

$$\hat{S}_{v,\alpha}|s\rangle = -\frac{(-1)^v}{2} \sum_{\beta} \delta_{\alpha\beta}|t_{\beta}\rangle, \quad (16a)$$

$$\hat{S}_{v,\alpha}|t_{\beta}\rangle = -\frac{1}{2} \left[2(-1)^v \delta_{\alpha\beta}|s\rangle - i \sum_{\delta} \epsilon_{\alpha\beta\delta}|t_{\delta}\rangle \right], \quad (16b)$$

where $v = \{1, 2\}$ labels the spin \hat{S}_1 and \hat{S}_2 , respectively. With these definitions, the matrices \hat{K} and \hat{M} in Eqs. (13a) and (13b) can be expressed in terms of these spin operators

$$\hat{K}_{\alpha} = -(\hat{S}_{1,\alpha} + \hat{S}_{2,\alpha}), \quad (17a)$$

$$\hat{M}_{\alpha} = \hat{S}_{1,\alpha} - \hat{S}_{2,\alpha}. \quad (17b)$$

The annihilation and creation operators of the harmonic oscillators can be expressed by position and momentum operators in the standard way

$$\hat{r}_{j,\alpha} = \frac{1}{\sqrt{2}}(\hat{a}_{j,\alpha}^{\dagger} + \hat{a}_{j,\alpha}), \quad (18a)$$

$$\hat{p}_{j,\alpha} = \frac{i}{\sqrt{2}}(\hat{a}_{j,\alpha}^{\dagger} - \hat{a}_{j,\alpha}). \quad (18b)$$

With these relations, the Hamiltonian in Eq. (10) can be rewritten into

$$\hat{\mathcal{H}}_{\text{eff}}^{\text{CS}} = -\frac{1}{\sqrt{2}}(\hat{S}_1 + \hat{S}_2) \cdot \hat{r}_1, \quad (19a)$$

$$\hat{\mathcal{H}}_{\text{eff}}^{\text{ch}} = \frac{1}{2} \sum_{j=1}^{N_{\text{tr}}} (\hat{S}_2 - \hat{S}_1) \cdot [(\chi_j \hat{r}_j + \eta_{j-1} \hat{r}_{j-1} + \eta_j \hat{r}_{j+1}) \times \hat{p}_j], \quad (19b)$$

$$\hat{\mathcal{H}}_{\text{eff}}^{\text{Z}} = h(\hat{S}_{1,z} + \hat{S}_{2,z}). \quad (19c)$$

Note that, except for the Zeeman term, the linear spin operators always occur in a product with bosonic operators, namely, position and momentum. Hence, it is not to be expected that a TWA treatment becomes rigorously exact.

The ensuing time evolution of the operators \hat{r} , \hat{p} , \hat{S}_1 , and \hat{S}_2 according to the Heisenberg equation of motion reads

$$\frac{d}{dt} \hat{r}_1 = \frac{\chi_1}{2} (\hat{S}_2 - \hat{S}_1) \times \hat{r}_1 + \frac{\eta_1}{2} (\hat{S}_2 - \hat{S}_1) \times \hat{r}_2, \quad (20a)$$

$$\begin{aligned} \frac{d}{dt} \hat{p}_1 &= \frac{\chi_1}{2} (\hat{S}_2 - \hat{S}_1) \times \hat{p}_1 + \frac{\eta_1}{2} (\hat{S}_2 - \hat{S}_1) \times \hat{p}_2 \\ &+ \frac{1}{\sqrt{2}} (\hat{S}_2 + \hat{S}_1), \end{aligned} \quad (20b)$$

for $j = 1$ while for general $j > 1$ we obtain

$$\begin{aligned} \frac{d}{dt} \hat{r}_j &= \frac{\chi_j}{2} (\hat{S}_2 - \hat{S}_1) \times \hat{r}_j + \frac{\eta_j}{2} (\hat{S}_2 - \hat{S}_1) \times \hat{r}_{j+1} \\ &+ \frac{\eta_{j-1}}{2} (\hat{S}_2 - \hat{S}_1) \times \hat{r}_{j-1}, \end{aligned} \quad (21a)$$

$$\begin{aligned} \frac{d}{dt} \hat{p}_j &= \frac{\chi_j}{2} (\hat{S}_2 - \hat{S}_1) \times \hat{p}_j + \frac{\eta_j}{2} (\hat{S}_2 - \hat{S}_1) \times \hat{p}_{j+1} \\ &+ \frac{\eta_{j-1}}{2} (\hat{S}_2 - \hat{S}_1) \times \hat{p}_{j-1}, \end{aligned} \quad (21b)$$

$$\begin{aligned} \frac{d}{dt} \hat{S}_v &= \frac{1}{\sqrt{2}} \hat{S}_v \times \hat{r}_1 - \frac{(-1)^v}{2} \hat{S}_v \times \sum_{j=1}^{N_{\text{tr}}} [\chi_j (\hat{r}_j \times \hat{p}_j) \\ &+ \eta_j (\hat{r}_{j+1} \times \hat{p}_j) + \eta_{j-1} (\hat{r}_{j-1} \times \hat{p}_j)] - h \hat{S}_v \times \bar{z}, \end{aligned} \quad (21c)$$

where we use $\bar{z} = (0 \ 0 \ 1)^{\top}$ in the last term of Eq. (21c). The sought autocorrelation (3) has been expressed for the effective model in Eq. (15c) which implies

$$S^{\alpha}(t) = \frac{1}{4} [(\hat{S}_1^{\alpha}(t) - \hat{S}_2^{\alpha}(t)) [(\hat{S}_1^{\alpha}(0) - \hat{S}_2^{\alpha}(0))]], \quad (22)$$

where the expectation value is taken with respect to the singlet state of spins 1 and 2 and the bosonic vacua.

Applying the standard TWA [52], the leading quantum corrections are recovered by averaging classical trajectories over distributions of initial conditions. The equations of motions (20) and (21) are viewed as differential equations for classical vectors starting from random initial conditions. For this purpose, normal distributions turned out to be particularly suitable for the initial conditions. Their benefit is that only the mean value and the variance are needed to determine the distribution fully. We choose a normal distribution for spin \hat{S}_1 with vanishing mean value and variance 1/4 for each component because $\langle \hat{S}^{\alpha} \rangle^2 = 1/4$ for $S = 1/2$ [53]. Since we mimic a singlet state, \hat{S}_2 is always chosen to be $-\hat{S}_1$ initially.

The position and momentum components are also drawn from a normal distribution with vanishing means. The variances are straightforwardly computed considering (18) yielding $\langle \hat{r}_{j,\alpha}^2 \rangle = 1/2 = \langle \hat{p}_{j,\alpha}^2 \rangle$. In practice, the time evolution of the central spin $S^{\alpha}(t)$ in Eq. (22) is calculated for configuration average over \mathcal{M} classical trajectories with \mathcal{M} being of the order of 10^6 – 10^7 to keep statistical errors low.

IV. NUMERICAL RESULTS

Here we show results of the two TWAs which are the protagonists of this study. The sTWA relies on the classical equations of motion for the spin operators of original CSM. Either each spin is tracked individually or a hierarchical chain representation is used. This does not make any discernible difference. We assume normal distributions of the initial conditions with zero expectation values and variances $\langle S_{\ell}^{\alpha} S_j^{\beta} \rangle = (1/4) \delta_{\alpha\beta} \delta_{\ell j}$ which have proven to yield reliable results [44,53,55]. In contrast, the bTWA solves the classical equations of motion for the effective model obtained by mapping the large spin bath to a bath of bosons.

Since J_Q is the energy unit in the numerical calculations, all times are measured in units of $1/J_Q$ having set \hbar to unity. The equations of motion have no lower or upper validity cutoff in time and, thus, can be applied to discuss the spin-spin correlation from $t = 0$ to $t \rightarrow \infty$. The effective number of coupled spins N_{eff} can also be chosen arbitrarily, but we keep in mind that the mapping to the effective model becomes exact in the limit of large spin baths. Further details of the effect of $N_{\text{eff}} = 2/\gamma$ in the bTWA are provided in Appendix A.

Figure 2 shows the autocorrelation of the central spin in absence of external magnetic fields. This is the central result of this paper. Clearly, we see that both approaches, sTWA and bTWA, are converged with respect to the truncation level j_{max} (for further details of the effect of j_{max} in the bTWA,

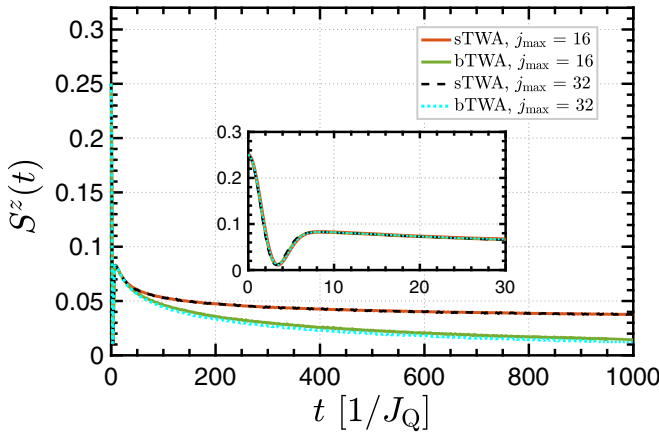


FIG. 2. Comparison of $S^z(t)$ obtained by sTWA and by bTWA for the truncation levels $j_{\max} = 16$ and 32 , fixed number of bath spins $N = 1000$, $\gamma = 0.01$ ($N_{\text{eff}} = 200$), and zero external magnetic field.

see Appendix B). The curves for $j_{\max} = 16$ do not differ discernibly from those for $j_{\max} = 32$. In the inset, we focus on the behavior on short to moderate times. Here the agreement between both approaches is very good. Since we know from previous studies [44] that the sTWA represents the quantum mechanical result very well, we deduce that the bTWA also works well in this temporal regime.

In the main panel of Fig. 2 we discern a significant discrepancy between the sTWA and the bTWA. This is quite surprising in view of the good agreement up to $t \approx 30/J_Q$. The convincing results obtained previously with sTWA [44] agrees with rigorous bounds [32,33] indicating a very slow decay of the autocorrelation. Thus, the conclusion is indicated that the bTWA does not approximate the long-time behavior of the CSM well. Still, it is (i) desirable to corroborate this conclusion further and (ii) important to understand whether the mapping to the effective bosonic model introduces the observed difference or whether it is the TWA applied to the bosonic model which induces this discrepancy.

Among the other approaches we employ the Bethe ansatz (BA) from which we use the data published in Ref. [33]. The BA is exact also for long times, but it can be handled only for a moderate number of bath spins. Second, in systematically controlled numerical density matrix renormalization group (DMRG) calculations we consider 4096 states [43] with a threshold of 0.001 for the accumulated discarded weight with second-order Trotter-Suzuki decomposition. The DMRG is not able to follow the dynamics for long times due to the rapid growth of entanglement. But up to $t \approx 50/J_Q$ it is reliable. The quantum mechanical evaluation of the iEoM up to $j_{\max} = 3$ with $\{181, 8, 1\}$ number of bosons, respectively, yields reliable data as well up to $t \approx 50/J_Q$ [56]. Data from these methods are depicted in Fig. 3 for two different sets of N and N_{eff} . The results from BA and DMRG agree very nicely for all times except for a tiny discrepancy at the minimum which we attribute to numerical inaccuracies. Note that the BA is evaluated based on Monte Carlo importance sampling implying small statistical fluctuations [30,31].

The iEoM approach, i.e., the quantum mechanical evaluation of the effective bosonic model also agrees well with the

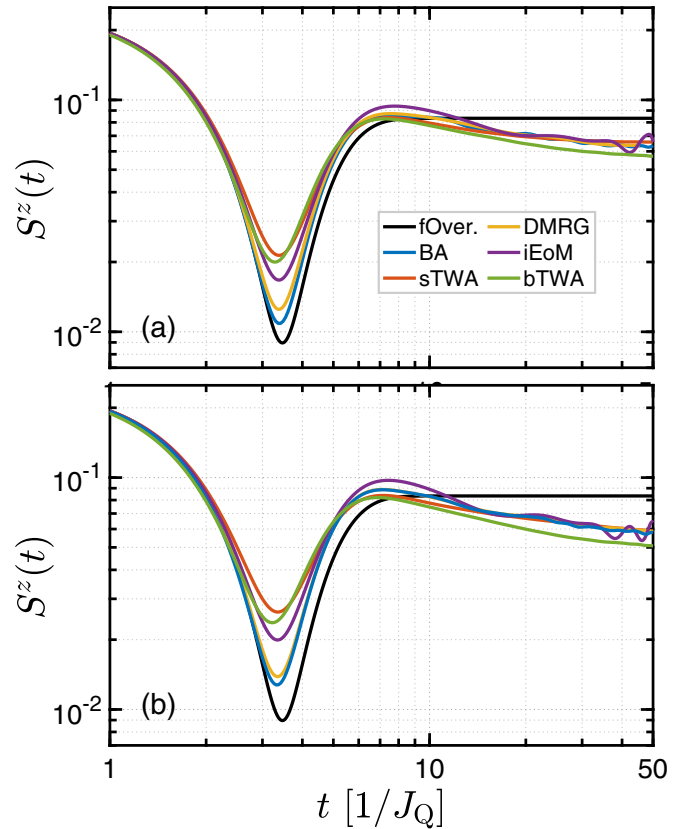


FIG. 3. Comparison of $S^z(t)$ from various approaches (BA, sTWA, DMRG, and iEoM) for fixed number of bath spins $N = 36$ and two different (a) $\gamma = 1/18$ ($N_{\text{eff}} = N = 36$) and (b) $\gamma = 1/12$ ($N_{\text{eff}} = 24$), see Appendix A for further details of the effect of γ in the bTWA. The analytic data for random static (frozen) Overhauser field (fOver) from Eq. (5) is included for comparison as well. In both iEoM and the TWAs, we use the truncation level $j_{\max} = 3$, see Appendix B for further details of the effect of j_{\max} in the bTWA.

BA and DMRG data, in particular, for the slow decay beyond $t \approx 6/J_Q$. Only the wiggles at $t \approx 50/J_Q$ indicate that the evaluation with the limited number of bosons is at the verge of its validity at this time. The discrepancies of the iEoM data to BA and DMRG data can be attributed to the fact that the mapping to the effective model is valid for large spin baths only, see the discussion in Ref. [56]. The sTWA data do not capture the minimum particularly well, but it agrees with the other approaches (BA, DMRG, iEoM) for longer times. The frozen Overhauser data from Eq. (5) are characterized by the constant plateau for long times because no dynamics of the Overhauser field is included.

What is the behavior of the data from bTWA? As we already saw in Fig. 2 for short and moderate times the agreement with sTWA and thus with the other data is good. In view of the long-time discrepancy observed in Fig. 2, we focus on the longer times beyond $20/J_Q$. We discern that the data from bTWA clearly lie below the other data which coincide very well (except for the frozen Overhauser curve). This observation corroborates our finding in Fig. 2 that the TWA applied to the effective bosonic model does not approximate the long-time behavior reliably. In addition, we learn that the

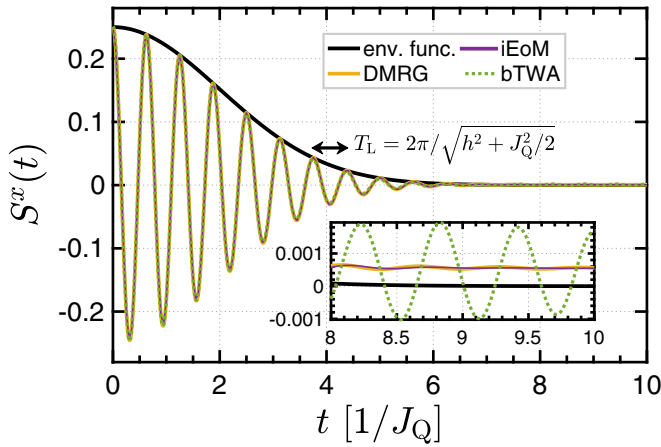


FIG. 4. Comparison of the x -component of the spin-spin autocorrelation obtained from DMRG, iEoM, and the bTWA at finite magnetic field $h/J_Q = 10$ along the z -direction. The parameters are $N = 500$, $j_{\max} = 3$, and $N_{\text{eff}} = 200$. The period of the Larmor precession is given by $T_L = 2\pi/\sqrt{h^2 + J_Q^2/2} \approx 0.63/J_Q$. The envelope function shown as black line is given by $S_{\text{env. func.}}(t) = \frac{1}{4} \exp(-J_Q^2 t^2/8)$. For the effect of h as well as the z -component of the spin-spin autocorrelation obtained from the bTWA, see Appendix C.

iEoM data, i.e., the quantum mechanical evaluation of the effective bosonic model, works fine at these times. Hence, Fig. 3 provides evidence that it is not the mapping to the effective bosonic bath which is responsible for the discrepancy, but the bTWA. Hence, the two questions posed above are answered.

This raises the question why the TWA is not as efficient as it is when applied directly to the spins. We do not yet have a concluding answer to this question but the hypothesis suggesting itself is the following. In the CSM, the conserved quantities of the *quantum* and of the *classical* model are the same which makes their dynamics very similar [32,33,44,75]. Clearly, a large number of conserved quantities hinders relaxation and thus explains that the autocorrelations relax slowly. In contrast, we presume that the conserved quantities of the *quantum* effective bosonic model and of this *classical* counterpart are not the same. This may explain why the semi-classical approach to the effective bosonic model leads to a deviating behavior. Note that this is no contradiction to the mapping [56] which is established on the quantum level only.

Finally, we address the CSM in a finite magnetic field which has been well investigated both theoretically and experimentally [76,77]. Data from DMRG, iEoM, and bTWA are depicted in Fig. 4 for a magnetic field in the z -direction. In the main panel, all data sets agree very well. All of them show the clear signature of Larmor precession with a period $T_L = 2\pi/\sqrt{h^2 + J_Q^2/2} \approx 0.63/J_Q$, cf. Refs. [27,44]. The envelope function of the Larmor precession is given by $S_{\text{env. func.}}(t) = \frac{1}{4} \exp(-J_Q^2 t^2/8)$ [38].

If we zoom far into the behavior at longer times after the signal has dephased, only minor discrepancies occur. This behavior is not unexpected since we learned already in the previous figures that the bTWA works well for times below $30/J_Q$. Hence the Larmor precessions and the Gaussian dephasing as shown by the black envelope function are retrieved

reliably. Only the small discrepancies at later times indicate that the approximate treatment is not perfect at long times. But in a magnetic field the signal has essentially vanished anyway in the long-time regime.

V. SUMMARY AND DISCUSSION

In this article, we theoretically studied the spin dynamics of the central spin in the central spin model (CSM). The CSM describes a so-called central spin coupled to spins in its environment in a star-like topology, i.e., without coupling between pairs of bath spins. This model is relevant for a plethora of physical systems where a small quantum system is coupled to a bath of other small quantum systems. A particularly interesting framework is the realization of quantum bits and their decoherence mechanisms due to their interaction with spin baths.

For many phenomena the long-time dynamics of large spin baths needs to be described reliably which poses an insurmountable challenge to brute force numerical approaches because of the exponential growth of the quantum Hilbert space. Hence, accurate, systematically controlled approximative approaches are needed. One of them is the mapping of the CSM with a large spin bath to a bath of bosons, i.e., to an effective bosonic model, including a four-dimensional impurity at the head of the chain. The bosonic degrees of freedom can be represented in a star topology or in a chain topology [56]. The chain topology has the advantage that one can add site by site of the chain to reach a reliable description up to longer and longer times. Thus, we employed this representation here. Still, the quantum mechanical evaluation of the resulting central spin dynamics is a great numerical challenge. For this reason, we studied in the present article how well a truncated Wigner approximation (TWA) for the bosonic effective model, dubbed bTWA, captures the sought dynamics. This kind of approximation averages correlations of classical trajectories over distributions of initial conditions and describes leading quantum correlations in this way [52].

We found that the bTWA works very nicely for short and moderate times if the spin bath is large. This condition on the size of the spin bath does not result from the TWA, but from the mapping of the CSM to the effective bosonic model. Only a few bosonic sites in the chain representation of the bosonic bath are necessary.

Much to our surprise, however, we found a qualitative discrepancy of the bTWA results compared to other approaches at long times. In this regime, the bTWA results display a significantly faster decay than the results by a direct application of the TWA to the CSM, dubbed sTWA. This discrepancy does not stem from the sTWA, but from the bTWA. Inspecting and comparing the behavior at moderate times where results from other approaches such as Bethe ansatz and DMRG are available indicates clearly that the correlations from bTWA are the deviating ones which are decaying too fast. Although the origin of this unexpected discrepancy is still unclear, we presume that the *classical* effective bosonic model, from which the trajectories are derived, that are averaged in bTWA over initial conditions, has different, probably less, conserved quantities than the quantum effective bosonic model or the original CSM. In contrast, the quantum and the classical CSM

share the same conserved quantities [32,33,44,75] so that their very similar behavior is plausible. Although we found this differing behavior for a particular model, the central spin model, we think it is fair to generalize it in the sense that the applicability of semi-classical approaches strongly depends on the set of variables which is employed to describe them. This conclusion is supported by other findings in the literature [53].

But clearly, further studies are called for to (i) identify unambiguously the origin of the discrepancy and (ii) to conceive reliable and efficient evaluation techniques for the effective bosonic model. One idea suggesting itself is to use numerical renormalization group techniques to evaluate its dynamics. Surely, this will enhance our understanding of decoherence and relaxation of small quantum systems suitable for realizing quantum bits or quantum sensors.

ACKNOWLEDGMENTS

We would like to thank P. Schering for useful discussions and for providing data of other approximate and exact approaches. This study was supported by the Deutsche Forschungsgemeinschaft (DFG, German Research Foundation) and the Russian Foundation for Basic Research in the International Collaborative Research Centre TRR 160 (GSU), by the DFG in project UH 90/14-1 (T.G. and G.S.U.) and by the Studienstiftung des Deutschen Volkes (K.B.). In addition, we also thank for the computing time provided on the Linux HPC cluster LiDO3 at TU Dortmund University. M.Y. greatly acknowledges the financial support by the National Science Foundation through Awards No. DMR-1945529, No. PHY-1607611, and No. NSF PHY1748958 as well as from the Welch Foundation through Award No. AT-2036-20200401.

APPENDIX A: EFFECT OF THE EFFECTIVE NUMBER OF BATH SPINS N_{eff} IN THE bTWA

The effective number of bath spins N_{eff} is one of the parameters influencing the minimum autocorrelation at intermediate timescales as well as the decoherence rates at long timescales. So, in the bTWA, it is important to investigate a range of N_{eff} for fixed $j_{\text{max}} = 3$ and $N = 500$ as depicted in Fig. 5, namely, $N_{\text{eff}} = 200, 100, 40, 25,$ and $20,$ respectively, corresponding to $\gamma = 0.01, 0.02, 0.05, 0.08,$ and $0.10.$ We obtain a square root behavior of $S_{\text{min}}^z(t_{\text{min}})$ as shown in the inset of Fig. 5 for increasing γ (decreasing N_{eff}). The coefficients $a = 0.285 \pm 0.005$ and $b = S_{\text{min}}^z(t_{\text{min}}J_Q = \sqrt{12})$ in the fitting function $f(\gamma) = a\sqrt{\gamma} + b$ depend on the set of the other parameters. The spin-spin autocorrelation for $\gamma = 0$ equals the one for the frozen Overhauser field with $S_{\text{min}}^z(t_{\text{min}}J_Q = \sqrt{12}) \simeq 0.009$ as a benchmark, see Eq. (5). This fact stems from the hyperfine coupling to the i th bath that is proportional to the square root of $\gamma.$

For larger values of γ beyond $\simeq 0.08$ we observe that the further changes of γ do not change the curves anymore, at least up to moderate times. This observation agrees with what was found by sTWA [54].

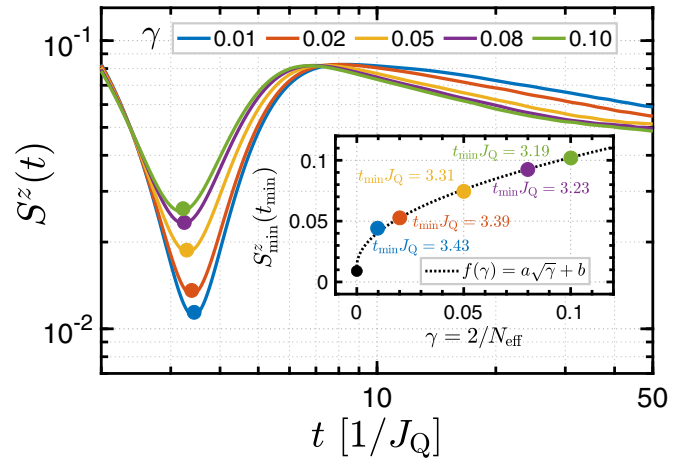


FIG. 5. The effect of the effective number of bath spins characterized by $\gamma = 2/N_{\text{eff}}$ in the bTWA on the spin-spin correlation at fixed $j_{\text{max}} = 3$ and $N = 500.$ The dotted fitting function in the inset is $f(\gamma) = a\sqrt{\gamma} + b$ with $a = 0.285 \pm 0.005$ and $b = S_{\text{min}}^z(t_{\text{min}}J_Q = \sqrt{12}),$ which confirms the square root proportionality of the minimum value of the correlation on $\gamma.$

APPENDIX B: EFFECT OF THE TRUNCATION LEVEL J_{max} IN THE bTWA

Here we study the effect of the maximum number of bosonic modes j_{max} in the bTWA, see Fig. 6, at a fixed number of bath spins $N = 500$ and $\gamma = 0.01$ (corresponding to $N_{\text{eff}} = 200).$ The curve for $j_{\text{max}} = 0$ shows the result for the frozen Overhauser field in Eq. (5). The curve for $j_{\text{max}} = 1$ induces only a very small temporal evolution of the Overhauser bath because the central spin is coupled only to a single harmonic oscillator which has a small effect on the position of the minimum. However, the long-time plateau value of the autocorrelation stays close to the frozen Overhauser field one for the studied times.

Taking into account a larger number of bosonic modes $j_{\text{max}} \geq 2,$ the difference between the static, frozen Overhauser result and the dynamic autocorrelations further increases. The

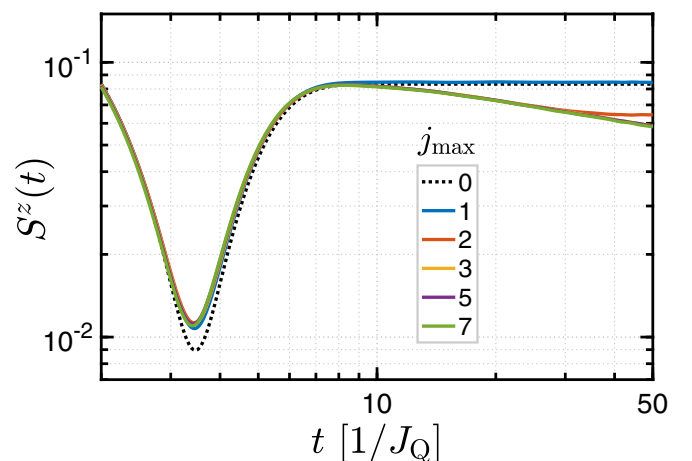


FIG. 6. The effect of truncation level characterized by j_{max} in the bTWA on the spin-spin autocorrelation at fixed $N = 500$ and $\gamma = 0.01$ ($N_{\text{eff}} = 200).$

frozen Overhauser curve (dashed line) is always below the other curves at short timescales. Clearly, the decay of the autocorrelation sets in only for $t > \tau$ after a specific time $\tau \simeq 10/J_Q$ which is almost independent of the set of parameters. For the shown time interval, the curves do not change significantly anymore for $j_{\max} \geq 3$ in accordance with previous results [56].

APPENDIX C: EFFECT OF THE EXTERNAL MAGNETIC FIELD ON THE SPIN-SPIN AUTOCORRELATION IN THE bTWA

In this Appendix, we address the role of a longitudinal magnetic field in the bTWA with the parameters $j_{\max} = 3$, $N = 500$, and $\gamma = 0.01$ ($N_{\text{eff}} = 200$) in Fig. 7. In this case, the solution of Eq. (21c) displays the precession of the central spin about the effective magnetic field, i.e., the Overhauser field plus the external magnetic field. Depending on the considered spin component, the Zeeman effect implies different behavior. For the z -autocorrelation of the central spin, Fig. 7(a), one finds that the decoherence rate is strongly suppressed by the magnetic field in a way that it approaches zero at strong fields where the spin-spin autocorrelation becomes almost time-independent and tends to take the initial value of $1/4$. This implies that the central spin polarization parallel to the external magnetic field is stabilized for $h \gg J_Q$.

Upon increasing magnetic field, the minimum of the longitudinal autocorrelation occurs earlier and earlier before it

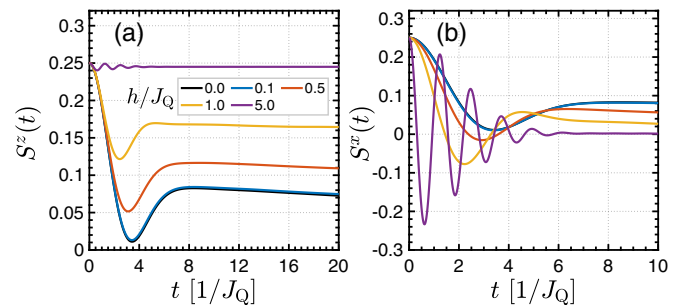


FIG. 7. The effect of the external longitudinal magnetic field on the (a) z -component and (b) x -component of the spin-spin autocorrelation at fixed $j_{\max} = 3$, $N = 500$, and $\gamma = 0.01$. The longitudinal central spin polarization is stabilized with the external longitudinal field and the amplitude of the oscillations is damped for increasing h such that, at strong-enough magnetic fields an almost time-independent autocorrelation function $S^z(t) \rightarrow 1/4$ results. In contrast, the transversal spin-spin autocorrelation displays prominent Larmor precession which quickly dephase due to the random Overhauser field.

is reduced to small oscillations and eventually to an almost constant plateau. In contrast to the longitudinal dynamics of the central spin, the transversal dynamics, Fig. 7(b), displays pronounced Larmor precessions with fast decreasing amplitude due to the dephasing induced by the fluctuations of the Overhauser field.

-
- [1] M. Gaudin, Diagonalisation d'une classe d'hamiltoniens de spin, *J. Phys. France* **37**, 1087 (1976).
- [2] M. Gaudin, *La fonction d'onde de Bethe*, Collection CEA: Série scientifique (Masson, Paris, 1983).
- [3] D. Loss and D. P. DiVincenzo, Quantum computation with quantum dots, *Phys. Rev. A* **57**, 120 (1998).
- [4] F. H. L. Koppens, K. C. Nowack, and L. M. K. Vandersypen, Spin Echo of a Single Electron Spin in a Quantum Dot, *Phys. Rev. Lett.* **100**, 236802 (2008).
- [5] W. A. Coish and D. Loss, Hyperfine interaction in a quantum dot: Non-Markovian electron spin dynamics, *Phys. Rev. B* **70**, 195340 (2004).
- [6] M. A. Nielsen and I. L. Chuang, *Quantum Computation and Quantum Information: 10th Anniversary Edition* (Cambridge University Press, Cambridge, England, 2010).
- [7] A. Greilich, S. E. Economou, S. Spatzek, D. R. Yakovlev, D. Reuter, A. D. Wieck, T. L. Reinecke, and M. Bayer, Ultrafast optical rotations of electron spins in quantum dots, *Nat. Phys.* **5**, 262 (2009).
- [8] S. E. Economou, L. J. Sham, Y. Wu, and D. G. Steel, Proposal for optical U(1) rotations of electron spin trapped in a quantum dot, *Phys. Rev. B* **74**, 205415 (2006).
- [9] S. G. Carter, A. Shabaev, S. E. Economou, T. A. Kennedy, A. S. Bracker, and T. L. Reinecke, Directing Nuclear Spin Flips in InAs Quantum Dots Using Detuned Optical Pulse Trains, *Phys. Rev. Lett.* **102**, 167403 (2009).
- [10] J. Schachenmayer, A. Pikovski, and A. M. Rey, Many-Body Quantum Spin Dynamics with Monte Carlo Trajectories on a Discrete Phase Space, *Phys. Rev. X* **5**, 011022 (2015).
- [11] A. Smith, M. S. Kim, F. Pollmann, and J. Knolle, Simulating quantum many-body dynamics on a current digital quantum computer, *npj Quantum Inf.* **5**, 106 (2019).
- [12] R.-B. Liu, W. Yao, and L. J. Sham, Quantum computing by optical control of electron spins, *Adv. Phys.* **59**, 703 (2010).
- [13] W. M. Witzel and S. Das Sarma, Quantum theory for electron spin decoherence induced by nuclear spin dynamics in semiconductor quantum computer architectures: Spectral diffusion of localized electron spins in the nuclear solid-state environment, *Phys. Rev. B* **74**, 035322 (2006).
- [14] P.-F. Braun, X. Marie, L. Lombez, B. Urbaszek, T. Amand, P. Renucci, V. K. Kalevich, K. V. Kavokin, O. Krebs, P. Voisin, and Y. Masumoto, Direct Observation of the Electron Spin Relaxation Induced by Nuclei in Quantum Dots, *Phys. Rev. Lett.* **94**, 116601 (2005).
- [15] D. S. Smirnov, E. A. Zhukov, D. R. Yakovlev, E. Kirstein, M. Bayer, and A. Greilich, Spin polarization recovery and Hanle effect for charge carriers interacting with nuclear spins in semiconductors, *Phys. Rev. B* **102**, 235413 (2020).
- [16] P. Schering, J. Hüdepohl, G. S. Uhrig, and B. Fauseweh, Nuclear frequency focusing in periodically pulsed semiconductor quantum dots described by infinite classical central spin models, *Phys. Rev. B* **98**, 024305 (2018).

- [17] A. Greilich, A. Shabaev, D. R. Yakovlev, A. L. Efros, I. A. Yugova, D. Reuter, A. D. Wieck, and M. Bayer, Nuclei-induced frequency focusing of electron spin coherence, *Science* **317**, 1896 (2007).
- [18] I. Kleinjohann, E. Evers, P. Schering, A. Greilich, G. S. Uhrig, M. Bayer, and F. B. Anders, Magnetic field dependence of the electron spin revival amplitude in periodically pulsed quantum dots, *Phys. Rev. B* **98**, 155318 (2018).
- [19] P. Schering, P. W. Scherer, and G. S. Uhrig, Interplay of spin mode locking and nuclei-induced frequency focusing in quantum dots, *Phys. Rev. B* **102**, 115301 (2020).
- [20] I. A. Yugova, M. M. Glazov, D. R. Yakovlev, A. A. Sokolova, and M. Bayer, Coherent spin dynamics of electrons and holes in semiconductor quantum wells and quantum dots under periodical optical excitation: Resonant spin amplification versus spin mode locking, *Phys. Rev. B* **85**, 125304 (2012).
- [21] D. S. Smirnov, E. A. Zhukov, E. Kirstein, D. R. Yakovlev, D. Reuter, A. D. Wieck, M. Bayer, A. Greilich, and M. M. Glazov, Theory of spin inertia in singly charged quantum dots, *Phys. Rev. B* **98**, 125306 (2018).
- [22] P. Schering, G. S. Uhrig, and D. S. Smirnov, Spin inertia and polarization recovery in quantum dots: Role of pumping strength and resonant spin amplification, *Phys. Rev. Res.* **1**, 033189 (2019).
- [23] M. M. Glazov and E. L. Ivchenko, Spin noise in quantum dot ensembles, *Phys. Rev. B* **86**, 115308 (2012).
- [24] N. Jäschke, F. B. Anders, and M. M. Glazov, Electron spin noise under the conditions of nuclei-induced frequency focusing, *Phys. Rev. B* **98**, 045307 (2018).
- [25] N. Fröhling, F. B. Anders, and M. Glazov, Nuclear spin noise in the central spin model, *Phys. Rev. B* **97**, 195311 (2018).
- [26] P. Glasenapp, D. S. Smirnov, A. Greilich, J. Hackmann, M. M. Glazov, F. B. Anders, and M. Bayer, Spin noise of electrons and holes in (In,Ga)As quantum dots: Experiment and theory, *Phys. Rev. B* **93**, 205429 (2016).
- [27] J. Hackmann and F. B. Anders, Spin noise in the anisotropic central spin model, *Phys. Rev. B* **89**, 045317 (2014).
- [28] A. M. Wojciechowski, M. Karadas, A. Huck, C. Osterkamp, S. Jankuhn, J. Meijer, F. Jelezko, and U. L. Andersen, Contributed review: Camera-limits for wide-field magnetic resonance imaging with a nitrogen-vacancy spin sensor, *Rev. Sci. Instrum.* **89**, 031501 (2018).
- [29] W. A. Coish and J. Baugh, Nuclear spins in nanostructures, *Physica Status Solidi (b)* **246**, 2203 (2009).
- [30] A. Faribault and D. Schuricht, Integrability-Based Analysis of the Hyperfine-Interaction-Induced Decoherence in Quantum Dots, *Phys. Rev. Lett.* **110**, 040405 (2013).
- [31] A. Faribault and D. Schuricht, Spin decoherence due to a randomly fluctuating spin bath, *Phys. Rev. B* **88**, 085323 (2013).
- [32] G. S. Uhrig, J. Hackmann, D. Stanek, J. Stolze, and F. B. Anders, Conservation laws protect dynamic spin correlations from decay: Limited role of integrability in the central spin model, *Phys. Rev. B* **90**, 060301(R) (2014).
- [33] U. Seifert, P. Bleicker, P. Schering, A. Faribault, and G. S. Uhrig, Persisting correlations of a central spin coupled to large spin baths, *Phys. Rev. B* **94**, 094308 (2016).
- [34] A. Melikidze, V. V. Dobrovitski, H. A. De Raedt, M. I. Katsnelson, and B. N. Harmon, Parity effects in spin decoherence, *Phys. Rev. B* **70**, 014435 (2004).
- [35] G. G. Kozlov, Exactly solvable spin dynamics of an electron coupled to a large number of nuclei; the electron-nuclear spin echo in a quantum dot, *J. Exp. Theor. Phys.* **105**, 803 (2007).
- [36] M. Bortz and J. Stolze, Spin and entanglement dynamics in the central-spin model with homogeneous couplings, *J. Stat. Mech.: Theory Exp.* (2007) P06018.
- [37] W. Yang, W.-L. Ma, and R.-B. Liu, Quantum many-body theory for electron spin decoherence in nanoscale nuclear spin baths, *Rep. Prog. Phys.* **80**, 016001 (2016).
- [38] I. A. Merkulov, A. L. Efros, and M. Rosen, Electron spin relaxation by nuclei in semiconductor quantum dots, *Phys. Rev. B* **65**, 205309 (2002).
- [39] A. V. Khaetskii, D. Loss, and L. Glazman, Electron Spin Decoherence in Quantum Dots due to Interaction with Nuclei, *Phys. Rev. Lett.* **88**, 186802 (2002).
- [40] W. Yao, R.-B. Liu, and L. J. Sham, Theory of electron spin decoherence by interacting nuclear spins in a quantum dot, *Phys. Rev. B* **74**, 195301 (2006).
- [41] E. Barnes, L. Cywiński, and S. Das Sarma, Nonperturbative Master Equation Solution of Central Spin Dephasing Dynamics, *Phys. Rev. Lett.* **109**, 140403 (2012).
- [42] W. M. Witzel and S. Das Sarma, Multiple-Pulse Coherence Enhancement of Solid State Spin Qubits, *Phys. Rev. Lett.* **98**, 077601 (2007).
- [43] D. Stanek, C. Raas, and G. S. Uhrig, Dynamics and decoherence in the central spin model in the low-field limit, *Phys. Rev. B* **88**, 155305 (2013).
- [44] D. Stanek, C. Raas, and G. S. Uhrig, From quantum-mechanical to classical dynamics in the central-spin model, *Phys. Rev. B* **90**, 064301 (2014).
- [45] V. W. Scarola, K. Park, and S. Das Sarma, Chirality in Quantum Computation with Spin Cluster Qubits, *Phys. Rev. Lett.* **93**, 120503 (2004).
- [46] S. K. Saikin, W. Yao, and L. J. Sham, Single-electron spin decoherence by nuclear spin bath: Linked-cluster expansion approach, *Phys. Rev. B* **75**, 125314 (2007).
- [47] W. Yang and R.-B. Liu, Quantum many-body theory of qubit decoherence in a finite-size spin bath, *Phys. Rev. B* **78**, 085315 (2008).
- [48] L. P. Lindoy and D. E. Manolopoulos, Simple and Accurate Method for Central Spin Problems, *Phys. Rev. Lett.* **120**, 220604 (2018).
- [49] J. Hackmann, P. Glasenapp, A. Greilich, M. Bayer, and F. B. Anders, Influence of the Nuclear Electric Quadrupolar Interaction on the Coherence Time of Hole and Electron Spins Confined in Semiconductor Quantum Dots, *Phys. Rev. Lett.* **115**, 207401 (2015).
- [50] D. S. Smirnov, V. N. Mantsevich, and M. M. Glazov, Theory of optically detected spin noise in nanosystems, *Phys. Usp.* **64**, 923 (2021).
- [51] D. A. Gangloff, G. Éthier-Majcher, C. Lang, E. V. Denning, J. H. Bodey, D. M. Jackson, E. Clarke, M. Hugues, C. L. Gall, and M. Atatüre, Quantum interface of an electron and a nuclear ensemble, *Science* **364**, 62 (2019).
- [52] A. Polkovnikov, Phase space representation of quantum dynamics, *Ann. Phys. (NY)* **325**, 1790 (2010).
- [53] S. M. Davidson and A. Polkovnikov, *SU(3)* Semiclassical Representation of Quantum Dynamics of Interacting Spins, *Phys. Rev. Lett.* **114**, 045701 (2015).

- [54] B. Fauseweh, P. Schering, J. Hüdepohl, and G. S. Uhrig, Efficient algorithms for the dynamics of large and infinite classical central spin models, *Phys. Rev. B* **96**, 054415 (2017).
- [55] B. Zhu, A. M. Rey, and J. Schachenmayer, A generalized phase space approach for solving quantum spin dynamics, *New J. Phys.* **21**, 082001 (2019).
- [56] R. Röhrig, P. Schering, L. B. Gravert, B. Fauseweh, and G. S. Uhrig, Quantum mechanical treatment of large spin baths, *Phys. Rev. B* **97**, 165431 (2018).
- [57] V. S. Zapasskii, A. Greilich, S. A. Crooker, Y. Li, G. G. Kozlov, D. R. Yakovlev, D. Reuter, A. D. Wieck, and M. Bayer, Optical Spectroscopy of Spin Noise, *Phys. Rev. Lett.* **110**, 176601 (2013).
- [58] S. A. Crooker, J. Brandt, C. Sandfort, A. Greilich, D. R. Yakovlev, D. Reuter, A. D. Wieck, and M. Bayer, Spin Noise of Electrons and Holes in Self-Assembled Quantum Dots, *Phys. Rev. Lett.* **104**, 036601 (2010).
- [59] J. Schliemann, A. Khaetskii, and D. Loss, Electron spin dynamics in quantum dots and related nanostructures due to hyperfine interaction with nuclei, *J. Phys.: Condens. Matter* **15**, R1809 (2003).
- [60] C. Bulutay, Quadrupolar spectra of nuclear spins in strained $\text{In}_x\text{Ga}_{1-x}\text{As}$ quantum dots, *Phys. Rev. B* **85**, 115313 (2012).
- [61] C. Bulutay, E. A. Chekhovich, and A. I. Tartakovskii, Nuclear magnetic resonance inverse spectra of InGaAs quantum dots: Atomistic level structural information, *Phys. Rev. B* **90**, 205425 (2014).
- [62] E. A. Chekhovich, K. V. Kavokin, J. Puebla, A. B. Krysa, M. Hopkinson, A. D. Andreev, A. M. Sanchez, R. Beanland, M. S. Skolnick, and A. I. Tartakovskii, Structural analysis of strained quantum dots using nuclear magnetic resonance, *Nat. Nanotechnol.* **7**, 646 (2012).
- [63] N. A. Sinitsyn, Y. Li, S. A. Crooker, A. Saxena, and D. L. Smith, Role of Nuclear Quadrupole Coupling on Decoherence and Relaxation of Central Spins in Quantum Dots, *Phys. Rev. Lett.* **109**, 166605 (2012).
- [64] K. C. Nowack, F. H. L. Koppens, Y. V. Nazarov, and L. M. K. Vandersypen, Coherent control of a single electron spin with electric fields, *Science* **318**, 1430 (2007).
- [65] M. J. Rančić and G. Burkard, Interplay of spin-orbit and hyperfine interactions in dynamical nuclear polarization in semiconductor quantum dots, *Phys. Rev. B* **90**, 245305 (2014).
- [66] A. V. Khaetskii and Y. V. Nazarov, Spin relaxation in semiconductor quantum dots, *Phys. Rev. B* **61**, 12639 (2000).
- [67] A. V. Khaetskii and Y. V. Nazarov, Spin-flip transitions between Zeeman sublevels in semiconductor quantum dots, *Phys. Rev. B* **64**, 125316 (2001).
- [68] V. N. Golovach, A. Khaetskii, and D. Loss, Phonon-Induced Decay of the Electron Spin in Quantum Dots, *Phys. Rev. Lett.* **93**, 016601 (2004).
- [69] L. B. Gravert, P. Lorenz, C. Nase, J. Stolze, and G. S. Uhrig, Increased coherence time in narrowed bath states in quantum dots, *Phys. Rev. B* **94**, 094416 (2016).
- [70] S. Lee, P. von Allmen, F. Oyafuso, G. Klimeck, and K. B. Whaley, Effect of electron-nuclear spin interactions for electron-spin qubits localized in InGaAs self-assembled quantum dots, *J. Appl. Phys.* **97**, 043706 (2005).
- [71] M. Y. Petrov, I. V. Ignatiev, S. V. Poltavtsev, A. Greilich, A. Bauschulte, D. R. Yakovlev, and M. Bayer, Effect of thermal annealing on the hyperfine interaction in InAs/GaAs quantum dots, *Phys. Rev. B* **78**, 045315 (2008).
- [72] B. Urbaszek, X. Marie, T. Amand, O. Krebs, P. Voisin, P. Malentinsky, A. Högele, and A. Imamoglu, Nuclear spin physics in quantum dots: An optical investigation, *Rev. Mod. Phys.* **85**, 79 (2013).
- [73] M. Abramowitz and I. A. Stegun, *Handbook of Mathematical Functions: With Formulas, Graphs, and Mathematical Tables*, Applied Mathematics Series (Dover, New York, 1965).
- [74] S. Sachdev and R. N. Bhatt, Bond-operator representation of quantum spins: Mean-field theory of frustrated quantum Heisenberg antiferromagnets, *Phys. Rev. B* **41**, 9323 (1990).
- [75] G. Chen, D. L. Bergman, and L. Balents, Semiclassical dynamics and long-time asymptotics of the central-spin problem in a quantum dot, *Phys. Rev. B* **76**, 045312 (2007).
- [76] W. Beugeling, G. S. Uhrig, and F. B. Anders, Quantum model for mode locking in pulsed semiconductor quantum dots, *Phys. Rev. B* **94**, 245308 (2016).
- [77] W. Beugeling, G. S. Uhrig, and F. B. Anders, Influence of the nuclear zeeman effect on mode locking in pulsed semiconductor quantum dots, *Phys. Rev. B* **96**, 115303 (2017).